Journal of Ovarian Research

RESEARCH

Open Access

B4GALT5 a sialylation-related genes associated with patient prognosis and immune microenvironment in ovarian cancer and pan-cancer

Di Wu[1], Li-yuan Sun[1], Xin-yu Chang[1] and Guang-mei Zhang[1*]

Abstract

Background Ovarian cancer (OC) is the predominant primary tumor in the human reproductive system. Abnormal sialylation has a significant impact on tumor development, metastasis, immune evasion, angiogenesis, and treatment resistance. B4GALT5, a gene associated with sialylation, plays a crucial role in ovarian cancer, and may potentially affect clinicopathological characteristics and prognosis.

Methods We conducted a comprehensive search across TIMER, GEPIA2, GeneMANIA, and Metascape to obtain transcription profiling data of ovarian cancer from The Cancer Genome Atlas (TCGA). The expression of B4GALT5 was test by immunohistochemistry. To investigate the impact of B4GALT5 on growth and programmed cell death in OC cells, we performed transwell assays and western blots.

Results The presence of B4GALT5 was strongly associated with an unfavorable outcome in OC. B4GALT5 significantly promoted the proliferation of OC cells. Upon analyzing gene ontology (GO) and Kyoto Encyclopedia of Genes and Genomes (KEGG), it was discovered that B4GALT5 played a crucial role in the extracellular matrix, particularly in collagen-containing structures, and exhibited correlations with ECM-receptor interactions, transcriptional dysregulation in cancer, as well as the interleukin-1 receptor signaling pathway. Furthermore, there is a clear link between B4GALT5 and the tumor immune microenvironment in OC. Moreover, B4GALT5 exhibits favorable expression levels across various types of cancers, including CHOL, KIRC, STAD and UCES.

Conclusion In conclusion, it is widely believed that B4GALT5 plays a pivotal role in the growth and progression of OC, with its heightened expression serving as an indicator of unfavorable outcomes. Moreover, B4GALT5 actively participates in shaping the cancer immune microenvironment within OC. This investigation has the potential to contribute significantly to a deeper understanding of the substantial involvement of B4GALT5 in human malignancies, particularly OCs.

Keywords B4GALT5, Ovarian cancer, Sialylation, Tumor microenvironment

*Correspondence:
Guang-mei Zhang
guangmeizhang@126.com
[1]Department of Obstetrics and Gynecology, The First Affiliated Hospital of Harbin Medical University, Harbin, Heilongjiang Province 150001, China

Introduction

Ovarian cancer is often diagnosed at an advanced stage, rendering it the most fatal among all gynecological cancers [1]. Despite the advancements made in chemotherapeutic drugs over the past few decades, there has been no discernible improvement in survival rates [2]. The primary therapeutic approaches for epithelial ovarian cancer include both debulking surgery and chemotherapy, with the status of debulking playing a crucial role in predicting patient outcomes [3]. Due to the highly metastatic nature of ovarian cancer, achieving complete tumor resection is rarely accomplished. Therefore, there is an urgent requirement for novel biomarkers or therapeutic targets to accurately predict prognosis, treatment response, and the occurrence of OC.

The regulation of posttranslational modifications is governed by families of sialyltransferases, transporters, and neuraminidases [4]. The preservation of cellular interactions through this mechanism plays a crucial biological role, which is implicated in the pathogenesis of various diseases, including cancer [5]. The sentence after revision: Diverse pathological disorders, including fatal embryonic development [6] and immune system abnormalities [7]. Maintaining cell-cell interactions is a critical biological function that performs an essential role. An increasing body of evidence suggests that tumors are characterized by aberrant sialylation [8]. According to mounting evidence, aberrant sialylation is a frequent occurrence in human cancers. Numerous studies have demonstrated the involvement of this particular enzyme in cancer development, as well as its role in tumor cell dissemination, invasion, immune evasion and treatment resistance [5]. Sialyltransferases have recently been proposed as potential targets for cancer treatment, due to their involvement in tumor progression. In order to augment the immune response against tumors, researchers have identified sialic acid-binding immunoglobulin-like lectins (Siglecs), including Siglec-5, -7, -9 and −10 [9]. Siglecs are widely expressed on various types of tumor-infiltrating cells, including T cells, neutrophils, and natural killer cells. For instance, through its interaction with CD24 expressed by tumors, Siglec-10 can inhibit tumor growth and improve survival rates [10]. Moreover, Siglec-15 has been identified as a cancer-associated receptor that suppresses the immune system and is exclusively expressed in the presence of programmed cell death ligand 1 (PD-L1), making it a potential alternative target for patients who are unresponsive to PD-1 therapy [11]. Additionally, Siglec-15 has been identified as a cancer-associated receptor that inhibits the immune system and is exclusively expressed in the presence of programmed cell death ligand 1 (PD-L1), rendering it a potential alternative target for patients who are unresponsive to PD-1 therapy [12, 13]. Sialyltransferases have predominantly been investigated in carcinoma research [14]. The study revealed a correlation between ST6 betagalactoside a-2,6-sialyltransferase 1 (ST6GAL1), an enzyme responsible for modifying N-acetyllactosamine, and the facilitation of metastasis as well as reduced survival rates in patients with OC [15]. Studies have demonstrated that artificial glycan ligands with a-2,6 sialylation exhibit high specificity towards Siglec-2, an immunotherapy target associated with B cells [16]. By utilizing biomarkers associated with sialylation-related molecules, it is thus possible to predict the survival outcomes in individuals diagnosed with ovarian cancer.

This study identified the mRNA associated with sialylation and pathways involving Siglec function in ovarian cancer patients. We successfully detected a B4GALT5 mRNA signature linked to sialylation in ovarian cancer and demonstrated its biological significance in ovarian cancer cells, as well as its expression across various types of cancers. Initially, we investigated the sialylation-associated markers in relation to clinical pathological characteristics, underlying mechanisms, somatic genetic alterations, and immune microenvironment factors among patients with ovarian cancer. Furthermore, our results demonstrate that B4GALT5, a sialylation-related signature of ovarian cancer, can serve as a novel biomarker for predicting mortality risks and elucidating critical signaling pathways. Furthermore, the involvement of B4GALT5 in personalized treatment for individuals diagnosed with ovarian cancer and other types of cancers is worth considering.

Materials and methods

Datasets

We obtained RNA sequencing (RNA-seq) data and corresponding clinical characteristics for 353 ovarian cancer patients from the TCGA repository at https://portal.gdc.cancer.gov/repository. We obtained RNA-seq data for 88 healthy human ovarian samples from the Genotype-Tissue Expression (GTEx) project (https://xenabrowser.net/datapages/). Gene expression profiles of an additional 1000 samples were acquired from the Gene Expression Omnibus database (GSE26712), and a validation cohort of 185 ovarian cancer patients was also included. The Molecular Signatures Database (MSigDB) was utilized to identify genes associated with sialylation (Supplementary Table S1).

Identification of differentially expressed sialylation-related genes

Table S1 presents a list of 109 sialylation-related genes that exhibit differential expression in the MSigDB. Due to limited availability of typical ovarian tissue information within the TCGA cohort, we further analyzed GTEx data from 88 healthy ovarian samples to identify differentially

expressed genes (DEGs) between normal and tumor tissues. The protein-protein interaction (PPI) network was constructed for differentially expressed genes (DEGs) with |log2(fold change)| > 1.5 and FDR < 0.05 using the Search Tool for the Retrieval of Interacting Genes (STRING).

Development and validation of the sialylation-related gene prognostic model

We utilized Cox regression analysis to evaluate the association between each gene and survival status in the TCGA cohort. Subsequently, a significance threshold of P-value 0.05 was applied to identify six genes significantly associated with survival. In order to construct the prognostic model and refine the candidate genes, we employed the LASSO Cox regression model (R package 'glmnet'). The seven genetic elements and their coefficients were retained, while the penalty parameter (λ) was determined based on the minimum requirements. Subsequently, the risk scores of the gene signature were calculated using the equation Risk score = (C coefficients, G gene expression level). TCGA OC patients were stratified into low- and high-risk subgroups according to their risk scores, and the Kaplan-Meier method was utilized to compare overall survival (OS) time between these two subgroups. Validation studies were performed using an ovarian cancer cohort obtained from the GEO database (GSE26712) and analyzed with R packages including 'survival', 'survminer', and 'timeROC'. The risk score was calculated based on the TCGA cohort, and to validate the accuracy of the gene model, subgroups in the GSE26712 cohort were further stratified according to low- and high-risk categories.

Functional enrichment analysis of the DEGs between the low- and high-risk groups

DEGs between low- and high-risk groups were selected based on specific criteria, requiring an absolute logarithmic fold change greater than 1.5 and a false discovery rate less than 0.05. The 'clusterProfiler' package was employed to analyze these DEGs.

Immune infiltrate analysis

CIBERSORT (R package 'CIBERSORT') was employed to calculate the relative ratios of immune cells infiltrating ovarian cancer. To estimate potential immune cell abundance, a reference set of 22 immune cell subtypes (LM22) with 1,000 permutations was utilized. Box plots were generated using the R package 'ggplot2' for visualization purposes to compare levels of immune cell infiltration between low- and high-risk groups.

Cell culture

For this study, we utilized two human ovarian cancer cell lines (SKOV3 and A2780) and one normal ovarian cell line (IOSE80). To verify their legitimacy, we examined the short tandem repeats (STR) of these cell lines. The cells were obtained from the BeNa Culture Collection in Shanghai, China and incubated at 37 °C with 5% CO_2 in RPMI-1640 medium supplemented with 10% fetal bovine serum (FBS; Gibco, Waltham, MA, USA).

Cell viability assay

CCK-8 Kits (Dojindo Molecular Technologies) were utilized to evaluate the cell viability of A2780 and SKOV3. After treatment with CCK-8, the cells were seeded in 96-well plates and incubated at 37 °C for a duration of 2 h. Subsequently, transfection with respective plasmids or siRNA was performed, and monitoring was conducted at specific time intervals (0 h, 24 h, 48 h, and 96 h). The OD values at 450 nm were determined using a Multimode Plate Reader from PerkinElmer in Germany.

Transwell assays

Polycarbonate transwells were utilized to seed a combined total of 104 A2780 and SKOV3 cells, which were subsequently transfected with either B4GALT5-si or control-si. During the 24-hour incubation period, cotton swabs were employed to eliminate non-migratory or invasive cells in the upper chambers. After fixation with 5% glutaraldehyde and staining with 0.5% crystal violet, we observed and quantified migrated cells on the lower membrane using a microscope located in Shangrao, China.

Flow cytometry

A2780 and SKOV3 cell lines were cultured in a 6-well plate for 48 h. The rate of cell apoptosis was evaluated using the FITC/PI Annexin V-fluorescein isothiocyanate (FITC) apoptosis kit and analyzed by flow cytometry using a FACS-can instrument (Becton Dickinson, San Jose, CA, USA) with CellQuest software (Becton Dickinson).

Acridine orange/ethidium bromide (AO/EB) assay

The apoptosis rate of A2780 and SKOV3 cells was evaluated using the AO/EB kit (Solarbio, Beijing, China). Following transfection with B4GALT5-si or control-si for 72 h, the cells were treated with 20 μl AO/EB (ratio = 1:1) in 1 ml PBS for a duration of 2 to 5 min. Subsequently, PBS was rinsed every 15 min. To visualize apoptotic cells, a Phoenix fluorescence microscope from Shangrao, China was employed.

Western blotting

Protein concentrations were determined using a conventional BCA technique after cell lysis in RIPA buffer supplemented with PMSF and a protease inhibitor cocktail for 30 min. The BCA kit from Solarbio (Beijing, China) was utilized for this purpose. Subsequently, the protein was separated via SDS-PAGE (Epizyme, Shanghai, China) and transferred onto polyvinylidene difluoride membranes from PALL (USA). After a 2-hour incubation at room temperature with 5% BSA, the membranes were subjected to an overnight incubation with specified primary antibodies (B4GALT5 and GAPDH, ZENBIO, Chengdu, China), followed by a 2-hour incubation with secondary antibodies labeled with HRP. The experiment employed an internal control, with GAPDH being utilized. Subsequently, the bands were visualized using an Infrared Imaging System by Bio-Rad, and densitometric analyses were conducted using Quantity One software (BioRad, USA).

Immunohistochemical staining

Approved by Ethics Committee of the first affiliated hospital of Harbin Medical University (Number: KY2022-115). In the same hospital, 57 patients with high-grade serous ovarian cancer and 12 patients with normal fallopian tubes were immunoassayed. An antigen retrieval procedure was carried out using citrate solution under high pressure after embedding tissues in paraffin, sectioning them, dewaxing, and rehydrating them. A 3% hydrogen peroxide solution was applied for 15 min to the sections, followed by a PBS wash and delineation using an immunohistochemical pen. Sections were blocked with 10% goat serum for 30 min, and overnight incubations with rabbit anti-B4GALT5 polyclonal antibody (1:50 dilution; Sangon, Shanghai, China) were performed. Diaminobenzidine (DAB) was used for color development after sections were washed with PBS and then incubated with secondary antibody (1:200 dilution, Sangon, Shanghai, China). In the next step, we stopped the reaction, stained the sections with hematoxylin, dehydrated them, and sealed them.

Statistical analysis

The statistical analyses were performed using R software (version 4.2.0). Kaplan-Meier analysis was employed to compare the occurrence of overall survival events and the probability of survival between low-risk and high-risk groups. The calibration curve analysis was performed based on R rms package. The decision curve analysis was performed based on R ggDCA package. Dates were analyzed using SPSS 21.0 and presented as mean ± standard error. Student's t-test was used to compare variances between two groups, while ANOVA was employed for multi-group comparisons. Statistical significance was set at $P<0.05$.

Results

Identification of DEGs between normal and tumor tissues

By analyzing data from the Genotype-Tissue Expression (GTEx) and The Cancer Genome Atlas (TCGA) databases, we have identified 34 differentially expressed genes (DEGs) that are associated with sialylation in 88 healthy and 353 cancerous tissues. Among the tumor group, 11 genes (GALNT17, GALNT10, ST3GAL5, ST6GALNAC6, HEXA, ST3GAL4, GALNT15, SIGLEC16, MAG, CD22 and SIGLEC11) were observed to be downregulated while 23 other genes (B3GNT3, AGRN, GALNT6, B3GNT2, GALNT12, GALNT3, ST6GAL1, ST6GALNAC2, B4GALT5, ITGB8, RTN4R, GALNT14, ST6GALNAC1, C1GALT1C1, ST6GALNAC5, GCNT1, S LC17A5, CHST6, ST8SIA4, CHST2, CHST1, GM2A, and NANP) were found to be enriched. Figure 1A depicts the RNA expression levels of these genes in the form of heatmaps, with green denoting low expression and red indicating high expression. In Fig. 1B, a minimum interaction score of 0.5 was required for PPI analysis of sialylation-related genes. After evaluation, we have identified GALNT17, GALNT10, ST3GAL5, ST6GALNAC6, HEXA, ST3GAL4, GALNT15, SIGLEC16, MAG, CD22, B3GNT3, GALNT6, B3GNT2, GALNT12, GALNT3, ST6GAL1, ST6GALNAC2, B4GALT5, RTN4R, GALNT14, ST6GALNAC1, C1GALT1C1, ST6GALNAC5, GCNT1, SCL17A5, CHST2, GM2A and NANP as the hub genes. All differentially expressed sialylation-related genes exhibit correlations as indicated in Fig. 1C with red representing positive correlations and blue representing negative correlations.

Tumor classification based on the DEGs

The correlation between the expression of 34 differentially expressed genes (DEGs) related to sialylation and ovarian cancer (OC) subtypes was investigated through a consensus clustering analysis using the TCGA cohort, which comprised 353 OC patients. As we increased the clustering factor from 2 to 9, we observed that intra-group correlations reached their peak while inter-group correlations reached their lowest point. By utilizing the expression levels of 34 differentially expressed genes (DEGs), it was possible to classify a cohort of 353 ovarian cancer (OC) patients into two distinct clusters (Fig. 2A). Furthermore, comparison of overall survival time between these two groups did not reveal any significant differences ($P=0.65$, Fig. 2B). As shown in Fig. 2C, there were observed DEGs that were significantly altered between the two clusters.

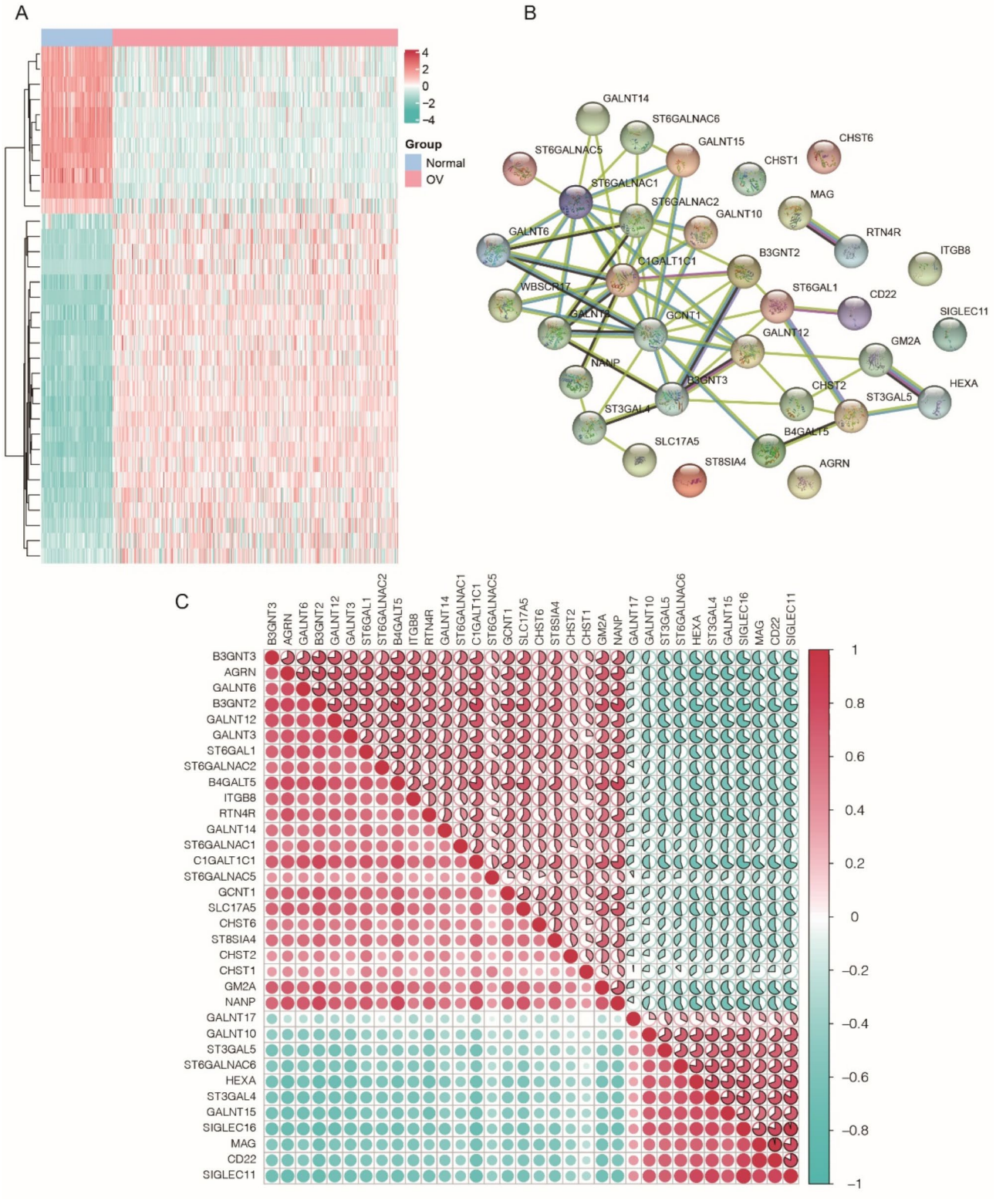

Fig. 1 Identification of DEGs between normal and tumor tissues. **(A)** The gene expression levels are visualized through heatmaps, where green indicates low expression and red indicates high expression. **(B)** Protein-protein interaction analysis was employed to investigate genes associated with sialylation. **(C)** The correlation network encompasses all differentially expressed genes related to sialylation, with positive correlations depicted in red and negative correlations in blue

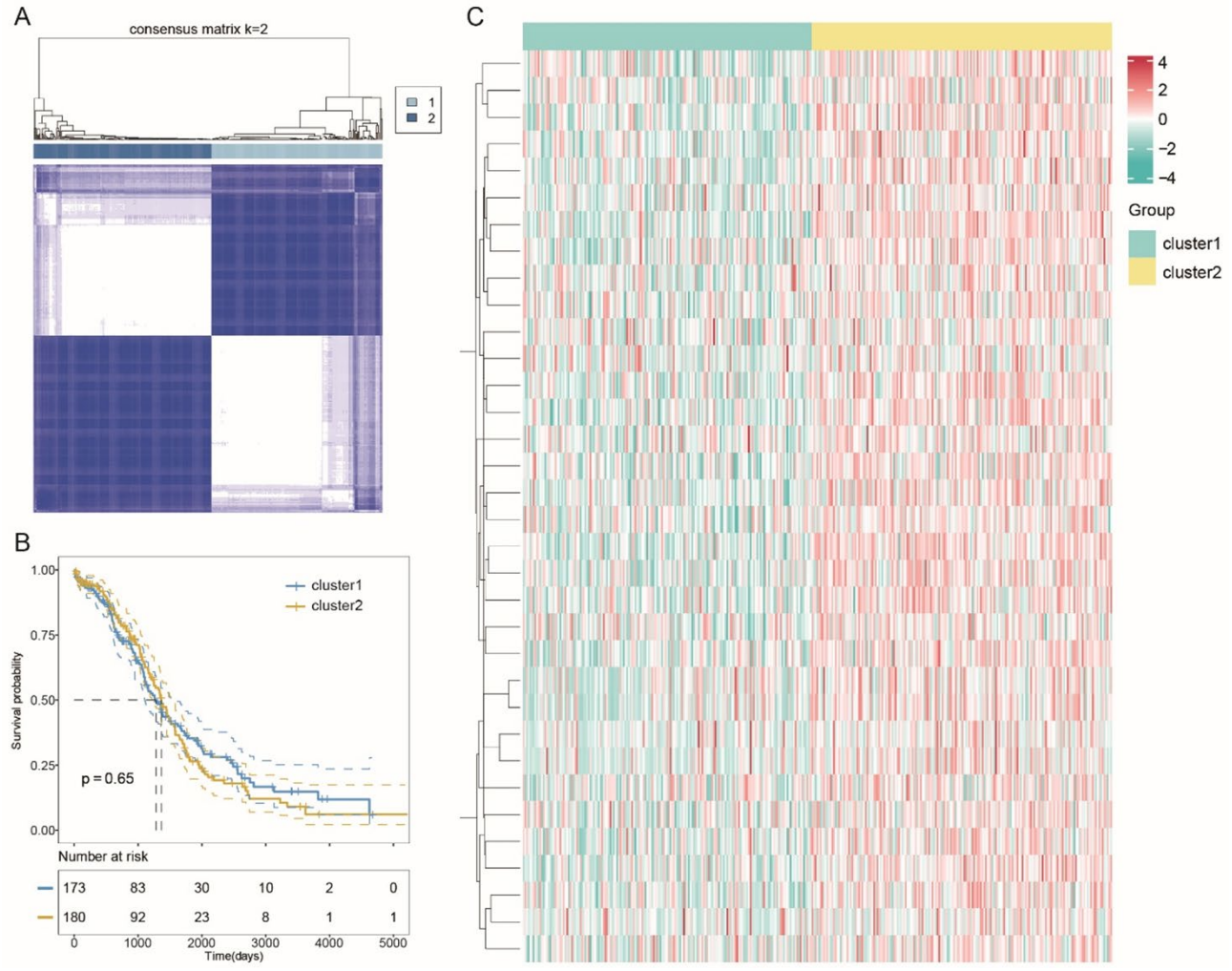

Fig. 2 Tumor classification based on the DEGs. **(A)** A consensus matrix was generated for k = 2. **(B)** depicting the survival without disease progression of two distinct cohorts in ovarian cancer. **(C)** Additionally, a heat map was constructed to visualize the expression patterns of fourteen differentially expressed genes (DEGs) within these two OC clusters

Development of a prognostic gene model in the TCGA cohort

The primary screening of genes associated with survival was conducted using univariate Cox regression analysis. Among the 7 genes (GALNT10, ST6GALNAC6, ITGB8, GALNT15, B4GALT5, and GALNT6) that met the $P<0.05$ criteria, 5 genes (GALNT10, ST6GALNAC6, ITGB8, GALNT15, and B4GALT5) exhibited an increased risk with hazard ratios (HRs) > 1; whereas one gene (GALNT6) showed a protective effect with HRs < 1 (Fig. 3A). A 6-gene signature was developed based on the results of LASSO Cox regression analysis, as illustrated in Fig. 3B and C. The risk score is computed using the following formula: Risk score = (0.1467235 * expression of ST6GALNAC6) + (0.0943779 * expression of B4GALT5) + (0.0804512 * expression of GALNT15) + (0.1041609 * expression of ITGB8) + (0.1208267 * expression of GALNT10) + (-0.147897 * expression of GALNT6). Based on this formula, a total of 353 patients were evenly stratified into low and high-risk subgroups, as illustrated in Fig. 3D. The number of fatalities in the high-risk category (Fig. 3E, located to the right of the dashed line) surpassed those observed in the low-risk categories. Notably, Fig. 3E demonstrates a significant contrast in overall survival duration between individuals classified as low-risk and high-risk ($P=0.00033$). The sensitivity and specificity of the prognostic model were evaluated by conducting a time-sensitive analysis of the receiver operating characteristic (ROC) curve. The AUC values for 1-year, 2-year, and 3-year survival were found to be 0.5618, 0.594, and 0.6202 respectively, as depicted in Fig. 3G. To validate the stability of the risk prediction model, we compared the predicted survival rates with the observed survival rates. The correlation between predicted and observed 1-year, 2-year and 3-year survival rates were plotted on calibration curves (Fig. 3H). Decision curve analysis was also

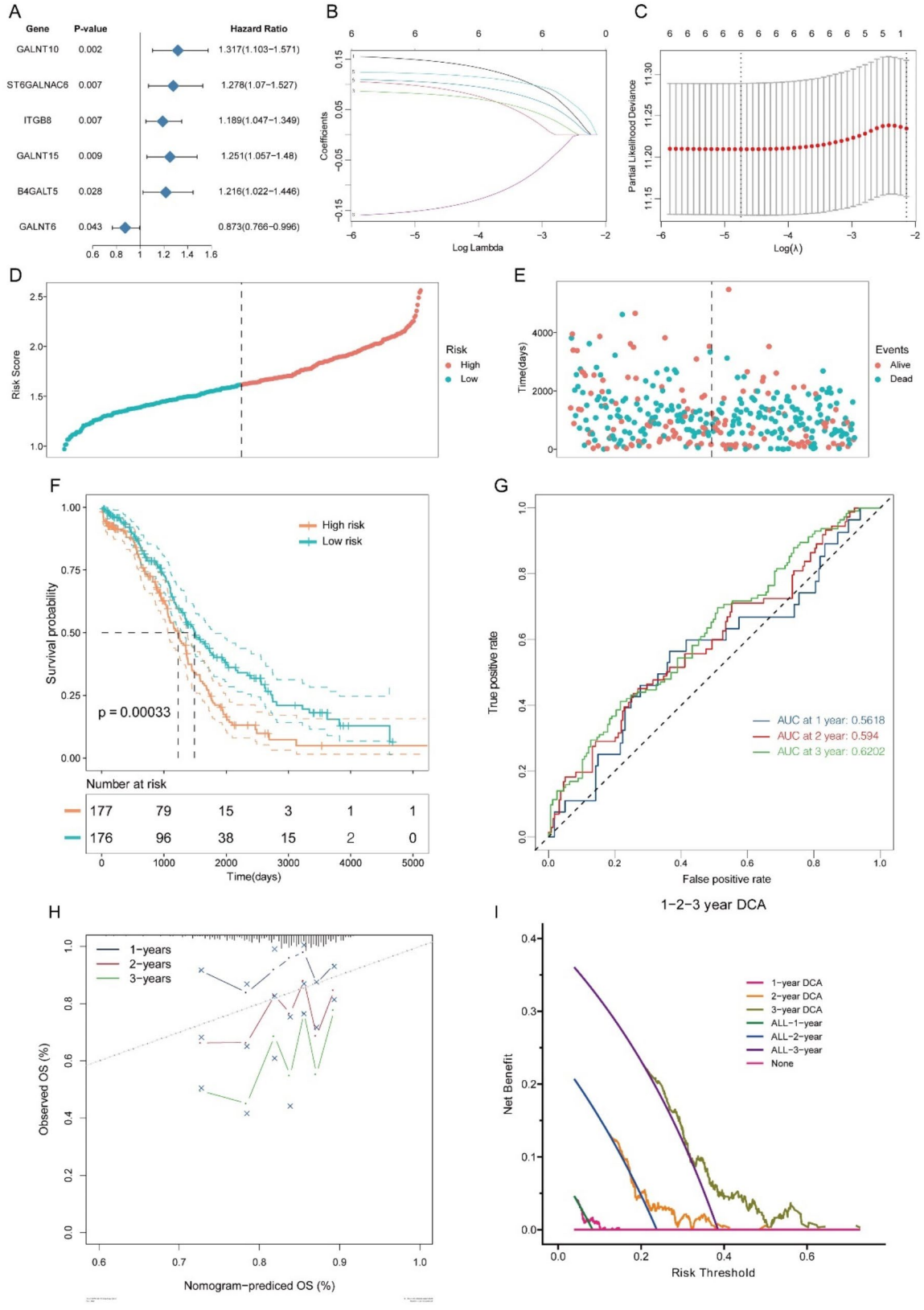

Fig. 3 (See legend on next page.)

(See figure on previous page.)

Fig. 3 Construction of risk signature in the TCGA cohort. **(A)** Univariate Cox regression analysis was performed for each gene related to sialylation, resulting in the identification of six genes with a significance level of $P < 0.05$. **(B-C)** LASSO regression was then conducted on these six genes associated with overall survival (OS), and parameter selection was carried out through cross-validation. **(D)** The sample distribution is based on the risk score. The survival status of each sample is displayed on the left for the low-risk population and on the right for the high-risk group. **(E)** Survival status for each sample (low risk population: left, high-risk group: right, respectively). **(F)** Kaplan-Meier plots demonstrate the overall survival of samples categorized into high- and low-risk groups. **(G)** ROC curves showcase the predictive capability of the risk score. **(H)** 1-year, 2-year and 3-year survival rates were plotted on calibration curves. **(I)** Decision curve analysis was also performed to assess the clinical utility of the risk model

performed to assess the clinical utility of the risk model. The relationship between risk thresholds and clinical utility is shown in Fig. 3I.

External validation of the risk signature

The validation group consisted of 185 individuals with ovarian cancer (OC) from the Gene Expression Omnibus (GEO) dataset (GSE26712). Based on the median risk score in the TCGA group, 34 individuals in the GEO group were identified as low-risk, while 151 individuals were classified as high-risk (Fig. 4A). Patients with a low-risk profile (positioned to the left of the dotted line in Fig. 4B) exhibited significantly lower mortality rates compared to those with a high-risk profile. Furthermore, Kaplan-Meier analysis revealed a notable distinction between the two risk categories ($P=0.0025$, as shown in Fig. 4C). After analyzing the ROC curve of the GEO cohort, we have identified that our model demonstrates robust predictability with an AUC of 0.6385 for one-year survival and 0.6095 for both two-year and three-year survival, as illustrated in Fig. 4D. Further, we compared the predicted survival rates with the observed survival rates to validate the stability of the risk prediction model. The correlation between predicted and observed 1-year, 2-year and 3-year survival rates were plotted on calibration curves (Fig. 4E). Decision curve analysis was also performed to assess the clinical utility of the risk model. The relationship between risk thresholds and clinical utility is shown in Fig. 4F.

Functional analyses based on the risk model

By utilizing the criteria of FDR 0.05 and |log2(Fold change) | > 1, we employed the "limma" R package to extract DEGs in order to investigate gene functions and pathways between subgroups. A total of 153 DEGs were identified between low- and high-risk groups within the TCGA cohort. In the TCGA cohort, a total of 153 differentially expressed genes (DEGs) were identified. Subsequently, a gene ontology (GO) enrichment analysis and Kyoto Encyclopedia of Genes and Genomes (KEGG) pathway analysis were conducted. The results revealed that the DEGs were primarily associated with immune receptor function, primary immunodeficiency, and chemokine binding (as illustrated in Fig. 5A and B).

Comparison of the immune activity between subgroups

Additionally, we performed a CIBERSORT analysis to compare the relative abundance of 22 distinct immune cell types between the low-risk and high-risk groups in both TCGA and GEO cohorts. Based on the TCGA cohort (Fig. 6A), it was observed that the high-risk subgroup exhibited a relatively diminished quantity of immune cells, particularly memory B cells, follicular helper T cells, resting NK cells, and activated NK cells when compared to the low-risk subgroup. Furthermore, an evaluation of the immune condition of the GEO group was conducted (Fig. 6B).

B4GALT5 is a potential biomarker and therapeutic target for OC

Previously, it was discovered that ovarian cancer (OC) has significant therapeutic value and biomarker potential associated with five genes (GALNT10, ST6GALNAC6, ITGB8, GALNT15, and B4GALT5). We utilized GEPIA tools to analyze the expression levels of these genes in the OC section of the TCGA dataset. Upon comparison between the OC patients and the control group, it was observed that GALNT10, ST6GALNAC6, and GALNT15 exhibited decreased levels. Conversely, ITGB8 and B4GALT5 showed elevated levels in patients with OC (Figure S1A-E). To the best of our knowledge, ITGB8 plays a significant role in the progression and treatment of ovarian cancer. For instance, Su C et al's study demonstrated that LncRNA TCF7 regulates ITGB8 to enhance viability, mobility, and stemness in epithelial ovarian cancer [17]. Huang B et al. demonstrated that the involvement of the miR-137/ITGB8 pathway in ovarian cancer's resistance to paclitaxel is modulated by the long noncoding RNA HULC [18]. High-grade serous ovarian cancer patients with elevated expression of Integrin Subunit beta 8 (ITGB8), as reported by He J et al., are more likely to experience unfavorable survival outcomes [19]. Based on the available evidence, ITGB8 is likely to have a significant impact on ovarian cancer. Although there are only limited reports on the presence of B4GALT5 in ovarian cancer patients, our study aims to investigate its function and potential impact. We test the expression of B4GALT5 in ovarian cancer patients by immunohistochemistry, our data shown the H-Score expression of B4GALT5 was increased in OC patients ($n=57$) compared normal group ($n=12$, Fig. 7A).

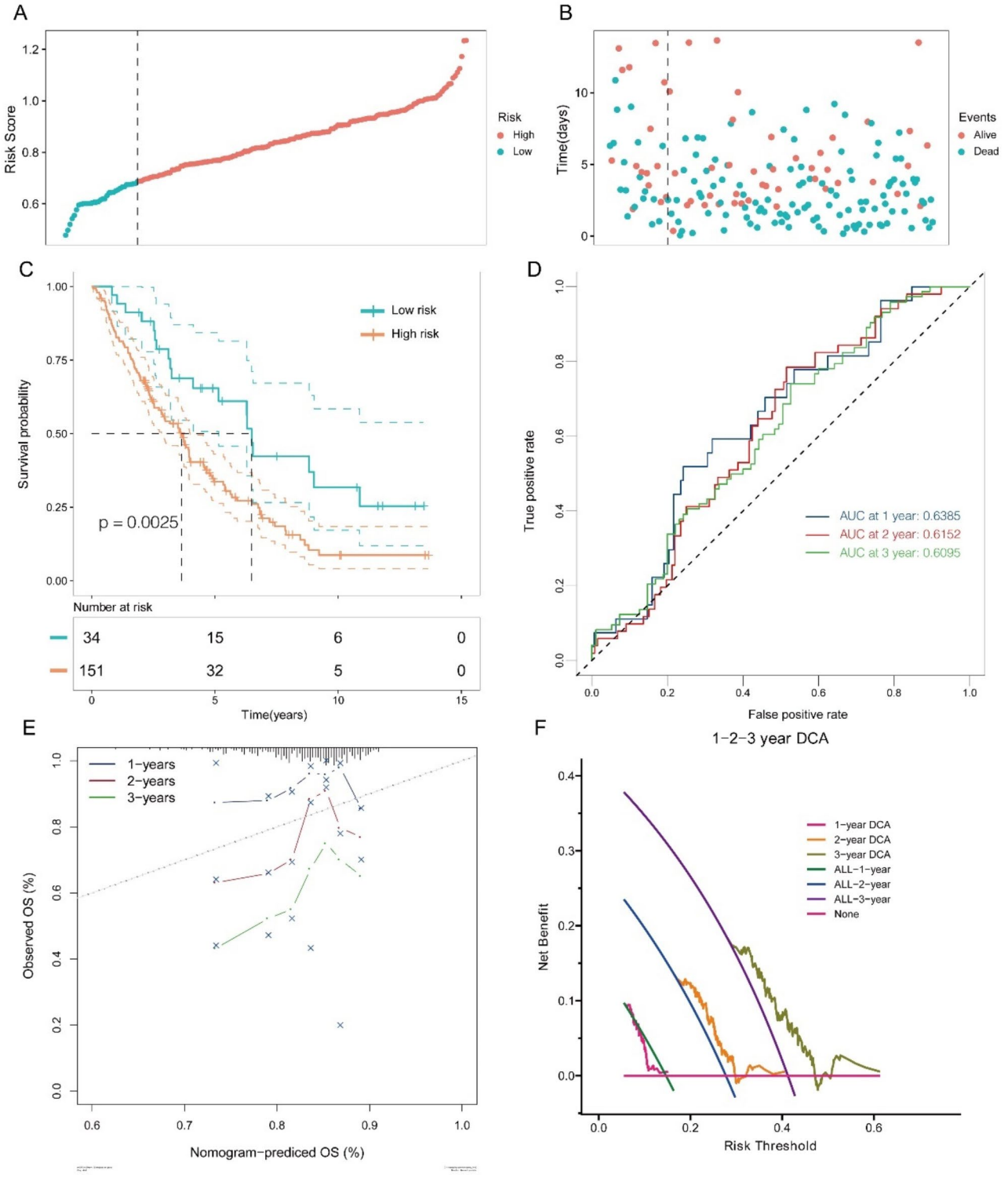

Fig. 4 Validation of the risk model in the GEO cohort. **(A)** Refinement of sample classification based on their level of risk. **(B)** The placement of each patient on the dotted line indicates their survival status, with those in the low-risk population positioned to the left and those in the high-risk population positioned to the right. **(C-D)** Kaplan-Meier curves were utilized to compare low- and high-risk groups, revealing temporal variations in the predictive efficacy of risk scores. **(E)** 1-year, 2-year and 3-year survival rates were plotted on calibration curves. **(F)** Decision curve analysis was also performed to assess the clinical utility of the risk model

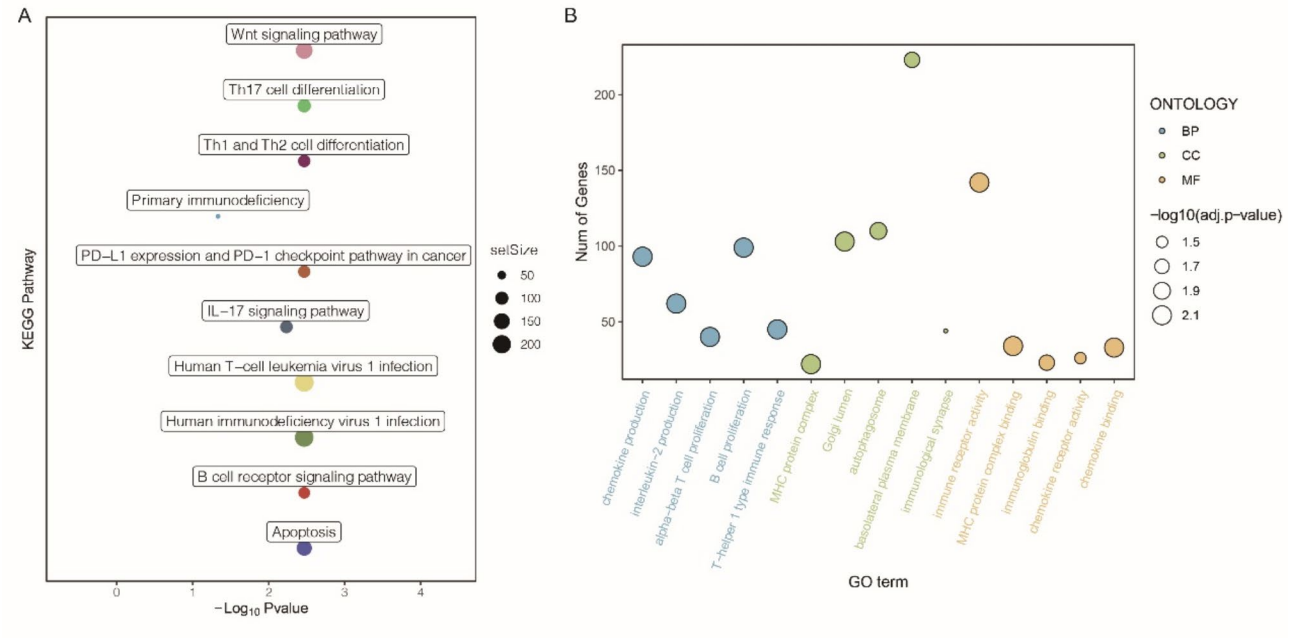

Fig. 5 Analysis of functional differences between two risk groups in the TCGA cohort based on DEGs. **(A)** Bubble graph for KEGG pathways. **(B)** Bubble graph for GO enrichment

B4GALT5 knockdown inhibited proliferation and invasion of OC cells

Two siRNAs were utilized to silence the expression of B4GALT5 in A2780 and SKOV3 cells for investigating its biological role. The Western blot analysis demonstrated that both siRNAs (Fig. 7B) effectively suppressed B4GALT5. In CCK-8 assays (Fig. 7C), depletion of B4GALT5 was found to reduce cell viability in A2780 and SKOV3 cells. Knockdown of B4GALT5 significantly reduced the apoptosis rate of OC cells, as demonstrated by flow cytometry and AO/EB staining (Fig. 7D-E). Conversely, we evaluated the invasion rate of OC cells following knockdown of B4GALT5 using Trans well assays (Fig. 7F). The data obtained from our study demonstrates that the silencing of B4GALT5 significantly suppresses the invasion rate of OC cells. Based on these findings, it can be concluded that B4GALT5-si not only inhibits the viability and invasion of OC cells but also induces apoptosis, indicating its potential as a promising target for OC treatment.

Expression patterns of B4GALT5 in pan-cancer

To investigate the expression of B4GALT5 in diverse tumors, we evaluated its protein levels across multiple publicly available databases. Our comprehensive analysis of the TGCA-GTEx database revealed distinct protein expression patterns of B4GALT5 in both healthy and tumor tissues. According to Fig. 8A, the expression of B4GALT5 protein varies across 33 human tissues, resulting in variations in protein quantification. Furthermore, differential expression of B4GALT5 was observed in 12 out of 33 tumors within the TCGA repository. However, with an increased number of normal samples in the GTEx database, B4GALT5 was found to be expressed in 27 out of 33% of tumors (Fig. 8B). Based on these findings, the varying expression patterns of B4GALT5 across different tumor types suggest its significant involvement in both tumor progression and onset.

Prognostic role of B4GALT5 in pan-cancer

To commence, we conducted a comprehensive analysis on the correlation between B4GALT5 expression and diverse cancer survival outcomes, encompassing OS, DSS, and PFI, across an array of cancer types. Based on survival analysis, increased expression of B4GALT5 was found to be associated with worse overall survival (OS), disease-specific survival (DSS), and progression-free interval (PFI) in four types of tumors: Cholangiocarcinoma (CHOL), Kidney renal clear cell carcinoma (KIRC), Stomach adenocarcinoma (STAD), and Uterine Corpus Endometrial Carcinoma (UCEC). This is illustrated in Fig. 9A-D.

Correlation of B4GALT5 and immune cells

In the context of pan-cancer, we examined the correlation between B4GALT5 expression and immune cells, given their pivotal role in immunotherapy. In 33 of the 39 tumor types analyzed, our findings revealed a significant correlation between B4GALT5 expression and the proportion of immune cells present within the tumor microenvironment, including neutrophils, B lineage and T cells, CD8+T cells, cytotoxic lymphocytes, myeloid

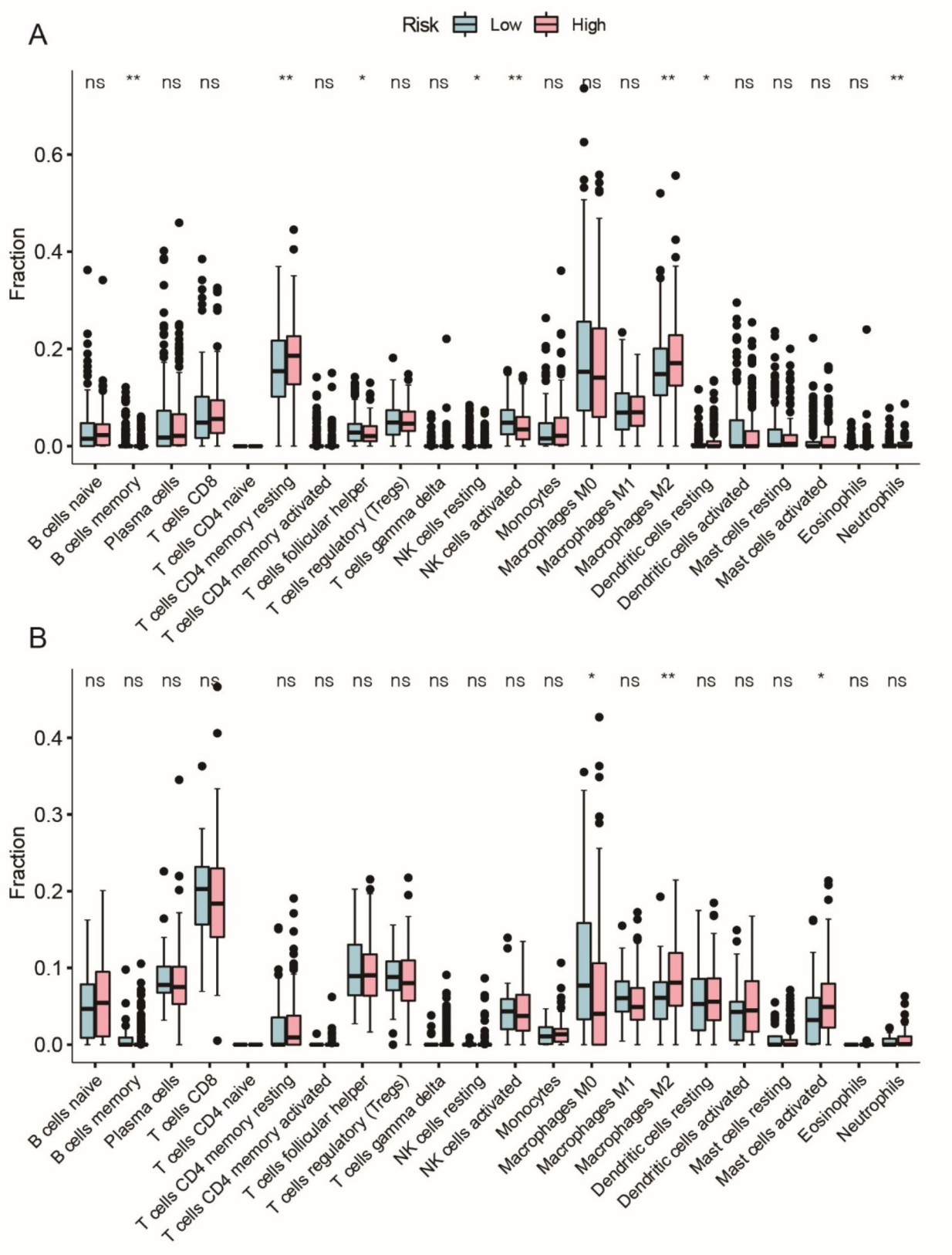

Fig. 6 The immune landscape between the two risk groups in the **(A)** TCGA and **(B)** GEO cohorts

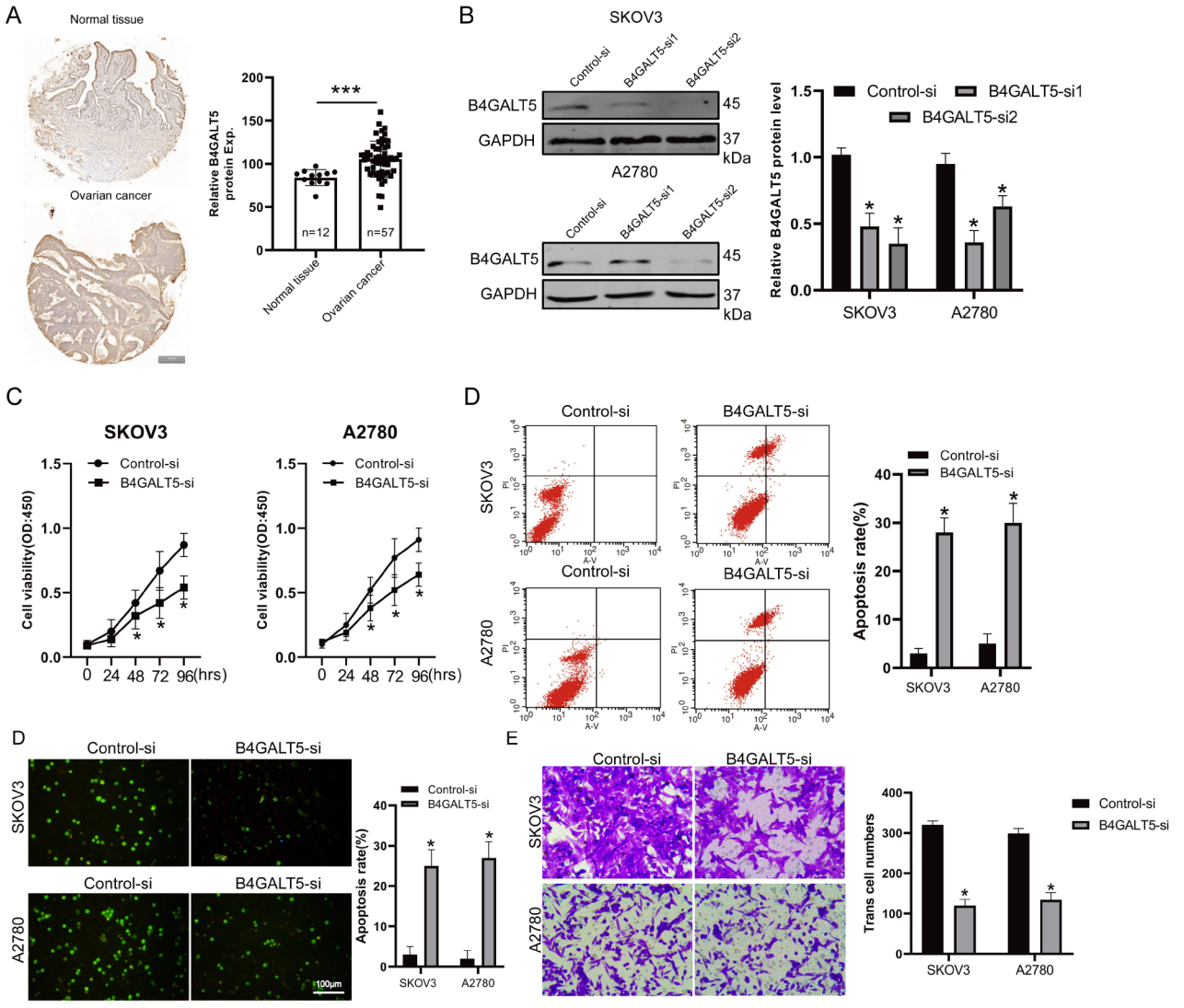

Fig. 7 B4GALT5 function loss experiment in vitro. **(A)** The expression of B4GALT5 in OC patient(Normal tissue $n = 12$, ovarian cancer $n = 57$). **(B)** The knockdown efficiency of B4GALT5 was assessed in both A2780 and SKOV3 cells using the western blotting technique. **(C)** The cell viability of A2780 and SKOV3 cells was evaluated utilizing the CCK-8 assay. **(D-E)** Flow cytometry and AO/EB staining were utilized to assess cellular apoptosis in A2780 and SKOV3 cells. **(F)** Trans well assay was used to compare B4GALT5 knockdown cells with control-si cells, and the results are presented as mean ± standard error of the mean. (*$P < 0.05$ compared to control-si group)

dendritic cells, monocytic lineage cells, fibroblasts, NK cells and endothelial cells. B4GALT5 expression in 23 tumors, such as UVM, DLBC, PRAD, KICH, LIHC, LGG, GBM, LAML, KIRP, ACC, UCS, SKCM, STAD, BLCAM, UCEC PCPG, OV, PAAD, KIRC, THCA, CESC, HNSC, and THYM, showed significant correlations with at least four ratios of immune cells. A strong association was observed between the proportion of immune cells and the expression of B4GALT5 in LIHC, THCA, KIRP, and KICH, as well as OV, KIRP, KICH, and OV (Fig. 10).

Discussion

The upregulation of sialic acid, referred to as hypersialylation, has been associated with Siglecs, resulting in tumor progression and compromised immune response [20]. Both natural killer cells and T cells that infiltrate tumors express siglecs, which are involved in immune system regulation as referenced [21]. Ongoing clinical trials are currently assessing the safety and tolerability of antibodies targeting Siglec-15, aiming to restore immune system homeostasis in patients with advanced cancer [22]. Uncertainty persists regarding the functions of mRNA in the intricate interplay between sialylation and Siglec, a specific RNA variant that regulates numerous pathways and has potential implications for early cancer

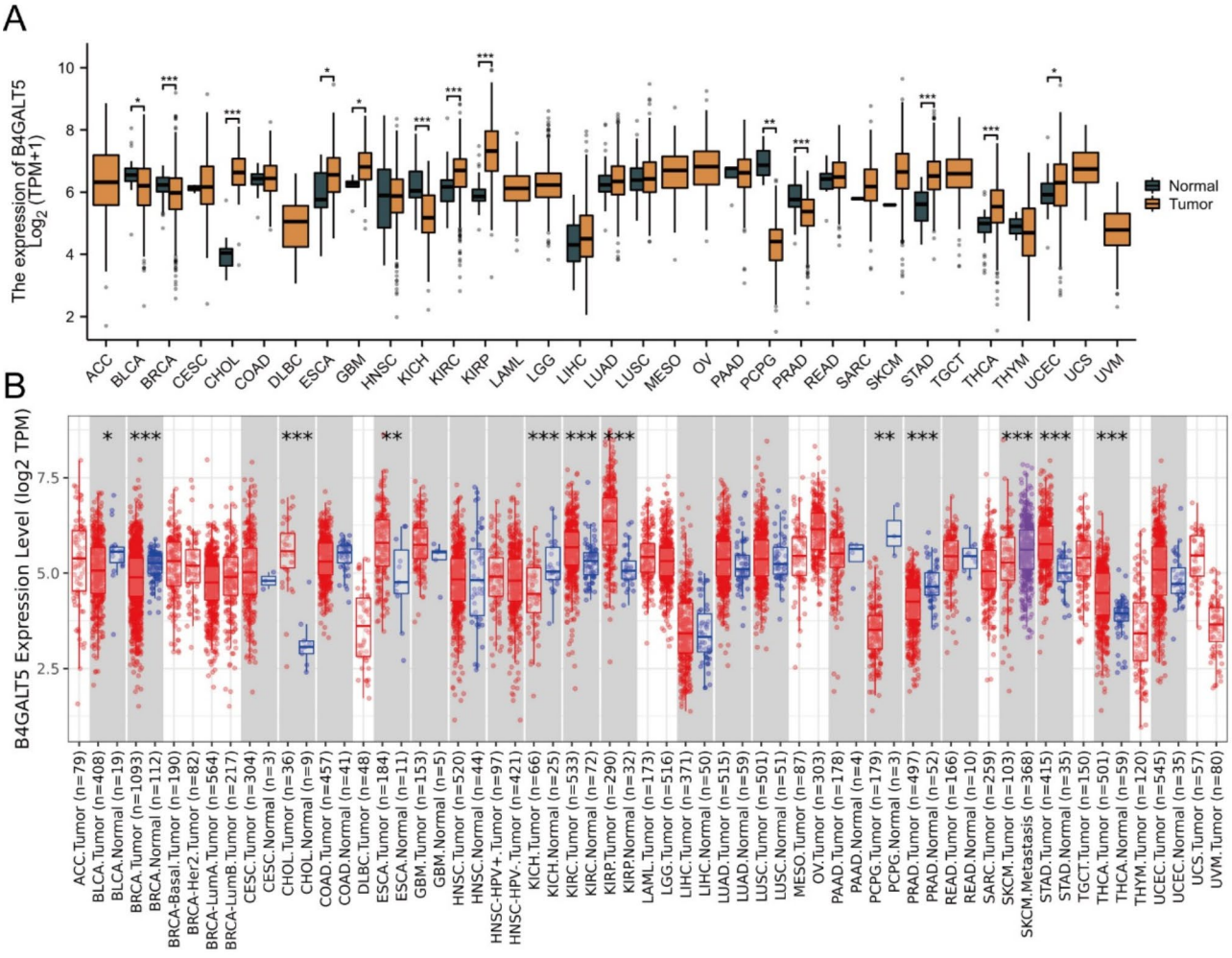

Fig. 8 Pan-cancer expression of B4GALT5. The expression level of B4GALT5 in normal tissues and tumor tissue from the TGCA-GTEx database **(A)** and in the TIMER database **(B)**. * $P < 0.05$; ** $P < 0.01$; *** $P < 0.001$

detection [23]. The existing evidence suggests that the utilization of diverse gene-related signatures with distinct biological functions is more efficacious in prognostication and customization of treatment plans [24]. Our objective was to investigate the clinical significance of a sialylation signature based on mRNA. A novel signature was developed using seven mRNAs that demonstrate a strong correlation with both the sialic acid and Siglec pathways.

Although there is limited evidence for cancer-related sialic acid-related genes, their incorporation into a 7-mRNA signature reveals a novel clinical significance. These 5 genetic markers can potentially aid in distinguishing patient prognosis and developing effective treatment strategies. Furthermore, the development of nomograms incorporating age, M stage, and risk score has demonstrated superior predictive accuracy compared to relying solely on clinical staging. To achieve this, it is imperative to optimize the current clinical staging classification [25]. Moreover, the 5-gene signature can calculate an independent risk score for ovarian cancer regardless of its major prognostic factors. To demonstrate the prognostic ability of this signature, we divided patients into high-risk and low-risk groups based on median values rather than optimal cutoff values due to subsequent factors. The median value, along with other robust methods, is commonly considered as an unsupervised approach. Numerous research studies generate mRNA signatures using median risk scores as a threshold. However, it should be noted that the optimal threshold values may vary across different groups and cannot be universally applied. Nonetheless, the use of median value as a cutoff can provide an unbiased approach for diverse datasets. Patients with a lower risk profile are expected to experience more favorable outcomes due to the enhanced strength of their fibroblasts and immune systems. The progression and metastasis of cancer are triggered by various components of the tumor stroma,

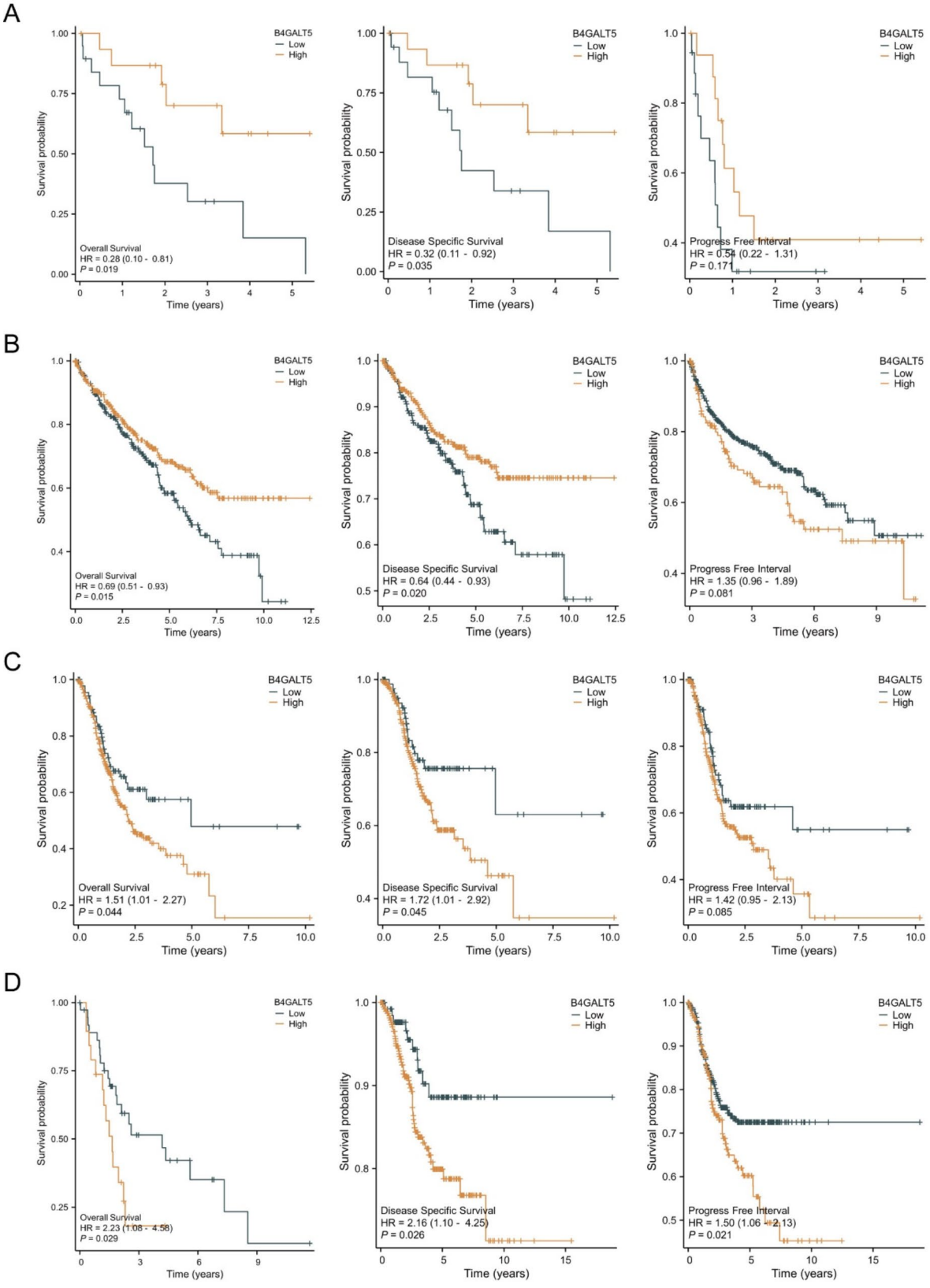

Fig. 9 The association of B4GALT5 with OS, DSS and PFI. Utilizing the TCGA database, we performed a survival analysis on diverse levels of B4GALT5 expression, with a focus on OS, DSS, and PFI outcomes. Specifically, this study investigated CHOL **(A)**, KIRC **(B)**, STAD **(C)**, and UCES **(D)** in patients exhibiting either elevated or reduced B4GALT5 expression

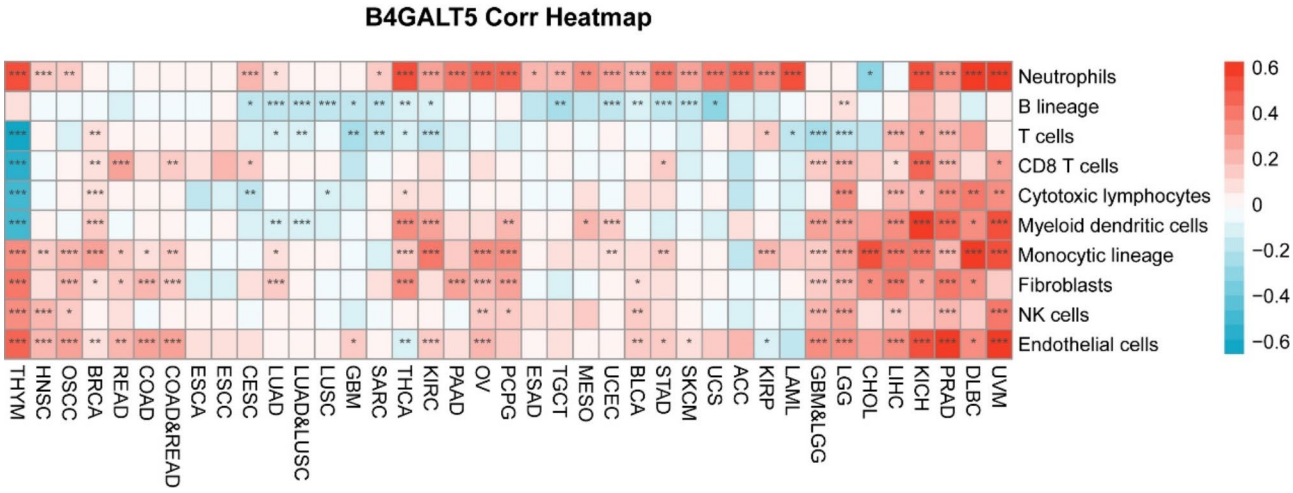

Fig. 10 The correlation of B4GALT5 expression and immune cell infiltration in pan-cancer * $P<0.05$; ** $P<0.01$; *** $P<0.001$; $^{ns}P>0.05$

including immune cells, activated fibroblasts, extracellular matrix, and other constituents of the basement membrane. Based on the findings of Epic and MCP-counter, it is suggested that cancer-associated fibroblasts may have a higher propensity to infiltrate patients at greater risk due to their ability to generate signals promoting tumor growth. Additionally, enrichment analysis revealed pathways such as wnt signaling, Th17 cell differentiation, Th1 and Th2 differentiation, and B cell reporter enriched in fibroblast-associated categories [26]. Using our signature, we can identify epigenetic alterations and the five sialylation-related genes identified may promote tumor growth by impairing the stromal microenvironment. The low-risk group exhibited enrichment of biological pathways and functional analyses associated with immune responses, including humoral immune responses, leukocyte migration, phagocytosis recognition, regulation of lymphocyte activation, and antigen binding as identified through pathway and functional enrichment analyses.

The B4GALT5 gene, also known as β-1, 4 galactosyltransferase V, belongs to the B4GALT family which comprises seven members [27]. One of the glycosyltransferases that has been extensively studied and garnered recent attention is B4GALT [27]. Studies suggest that galactosyltransferases exert a significant influence on embryonic development, neurological maturation, immune and inflammatory responses, tumorigenesis, as well as various other biological processes and pathologies [28]. However, The function of individuals within the galactosyltransferase group is contingent upon their substrate specificity and tissue distribution [29]. Currently, the functionality of β4Ga1T1 is the most extensively researched aspect, with β4Ga1T5 being the next in line for investigation [30]. Our findings suggest that TCGA expression data has the potential to determine clinical therapy outcomes and guide drug selection for patients with varying sialylation-related gene signature scores in the future. To validate the role and impacts of B4GALT5, it is necessary to consider the distinction between two types of ovarian cancer cells, namely A2780 and SKOV3. To investigate the underlying cause of the comparatively reduced expression of B4GALT5 in A2780 and SKOV3 cells, we conducted transfection experiments with B4GALT5-si and analyzed cell viability and apoptosis rates. Our findings demonstrate that B4GALT5 exhibits a favorable anti-ovarian cancer effect in *vitro*. Moreover, inhibition of B4GALT5 effectively reduces the migration rate of ovarian cancer cells.

Conclusion

The prognostic significance and functional role of B4GALT5, a critical regulator of OC, were investigated in this study, along with the expression patterns of genes associated with sialylation in OC. Our study demonstrated that B4GALT5 serves as a valuable predictive biomarker for identifying instances of ovarian cancer and holds potential for therapeutic intervention.

Supplementary Information

The online version contains supplementary material available at https://doi.org/10.1186/s13048-024-01503-3.

Supplementary Material 1

Acknowledgements
We appreciate Mr. Hui SUN with the help of Bioinformatics analysis.

Author contributions
DW. and LY S. wrote the main manuscript text and DW, XY and GM Z prepared all figures. All authors reviewed the manuscript.

Funding
Postdoctoral Science Foundation of Heilongjiang Province (LBH-Z18161). Research and Innovation Fund of the First Affiliated Hospital of Harbin Medical University (2021B16).

Data availability
No datasets were generated or analysed during the current study.

Declarations

Competing interests
The authors declare no competing interests.

Received: 19 February 2024 / Accepted: 19 August 2024
Published online: 29 August 2024

References

1. Morand S, Devanaboyina M, Staats H, Stanbery L, Nemunaitis J. Ovarian Cancer Immunotherapy and Personalized Medicine. Int J Mol Sci 2021, 22(12).
2. Penny SM. Ovarian Cancer: an overview. Radiol Technol. 2020;91(6):561–75.
3. Eisenhauer EA. Real-world evidence in the treatment of ovarian cancer. Ann Oncol. 2017;28(suppl8):viii61–5.
4. Lee WL, Wang PH. Aberrant sialylation in ovarian cancers. J Chin Med Assoc. 2020;83(4):337–44.
5. Dobie C, Skropeta D. Insights into the role of sialylation in cancer progression and metastasis. Br J Cancer. 2021;124(1):76–90.
6. Li F, Ding J. Sialylation is involved in cell fate decision during development, reprogramming and cancer progression. Protein Cell. 2019;10(8):550–65.
7. Bordron A, Morel M, Bagacean C, Dueymes M, Pochard P, Harduin-Lepers A, Jamin C, Pers JO. Hyposialylation must be considered to develop future therapies in Autoimmune diseases. Int J Mol Sci 2021, 22(7).
8. Munkley J. Aberrant sialylation in Cancer: Therapeutic opportunities. Cancers (Basel) 2022, 14(17).
9. Rodriguez E, Boelaars K, Brown K, Eveline Li RJ, Kruijssen L, Bruijns SCM, van Ee T, Schetters STT, Crommentuijn MHW, van der Horst JC, et al. Sialic acids in pancreatic cancer cells drive tumour-associated macrophage differentiation via the Siglec receptors Siglec-7 and Siglec-9. Nat Commun. 2021;12(1):1270.
10. Barkal AA, Brewer RE, Markovic M, Kowarsky M, Barkal SA, Zaro BW, Krishnan V, Hatakeyama J, Dorigo O, Barkal LJ, et al. CD24 signalling through macrophage Siglec-10 is a target for cancer immunotherapy. Nature. 2019;572(7769):392–6.
11. Wang J, Sun J, Liu LN, Flies DB, Nie X, Toki M, Zhang J, Song C, Zarr M, Zhou X, et al. Siglec-15 as an immune suppressor and potential target for normalization cancer immunotherapy. Nat Med. 2019;25(4):656–66.
12. Sun J, Lu Q, Sanmamed MF, Wang J. Siglec-15 as an emerging target for next-generation Cancer Immunotherapy. Clin Cancer Res. 2021;27(3):680–8.
13. Egan H, Treacy O, Lynch K, Leonard NA, O'Malley G, Reidy E, O'Neill A, Corry SM, De Veirman K, Vanderkerken K et al. Targeting stromal cell sialylation reverses T cell-mediated immunosuppression in the tumor microenvironment. Cell Rep 2023:112475.
14. Wu X, Zhao J, Ruan Y, Sun L, Xu C, Jiang H. Sialyltransferase ST3GAL1 promotes cell migration, invasion, and TGF-beta1-induced EMT and confers paclitaxel resistance in ovarian cancer. Cell Death Dis. 2018;9(11):1102.
15. Wichert B, Milde-Langosch K, Galatenko V, Schmalfeldt B, Oliveira-Ferrer L. Prognostic role of the sialyltransferase ST6GAL1 in ovarian cancer. Glycobiology. 2018;28(11):898–903.
16. Irons EE, Punch PR, Lau JTY. Blood-borne ST6GAL1 regulates Immunoglobulin Production in B cells. Front Immunol. 2020;11:617.
17. Su C, Huang K. LncRNA TCF7 promotes epithelial ovarian Cancer viability, mobility and stemness via regulating ITGB8. Front Oncol. 2021;11:649655.
18. Huang B, Wei M, Hong L. Long noncoding RNA HULC contributes to paclitaxel resistance in ovarian cancer via miR-137/ITGB8 axis. Open Life Sci. 2021;16(1):667–81.
19. He J, Liu Y, Zhang L, Zhang H. Integrin subunit beta 8 (ITGB8) upregulation is an independent predictor of unfavorable survival of high-Grade Serous Ovarian Carcinoma patients. Med Sci Monit. 2018;24:8933–40.
20. Stanczak MA, Rodrigues Mantuano N, Kirchhammer N, Sanin DE, Jacob F, Coelho R, Everest-Dass AV, Wang J, Trefny MP, Monaco G, et al. Targeting cancer glycosylation repolarizes tumor-associated macrophages allowing effective immune checkpoint blockade. Sci Transl Med. 2022;14(669):eabj1270.
21. Wu Y, Huang W, Xie Y, Wang C, Luo N, Chen Y, Wang L, Cheng Z, Gao Z, Liu S. Siglec-9, a putative Immune checkpoint marker for Cancer Progression Across multiple Cancer types. Front Mol Biosci. 2022;9:743515.
22. Zhao Y, Lv J, Zhang H, Xie J, Dai H, Zhang X. Gene expression profiles analyzed using integrating RNA sequencing, and microarray reveals increased inflammatory response, proliferation, and Osteoclastogenesis in Pigmented Villonodular Synovitis. Front Immunol. 2021;12:665442.
23. Griciuc A, Federico AN, Natasan J, Forte AM, McGinty D, Nguyen H, Volak A, LeRoy S, Gandhi S, Lerner EP, et al. Gene therapy for Alzheimer's disease targeting CD33 reduces amyloid beta accumulation and neuroinflammation. Hum Mol Genet. 2020;29(17):2920–35.
24. Nebgen DR, Lu KH, Bast RC Jr. Novel approaches to Ovarian Cancer Screening. Curr Oncol Rep. 2019;21(8):75.
25. Ramalingam P. Morphologic, immunophenotypic, and molecular features of epithelial ovarian Cancer. Oncol (Williston Park). 2016;30(2):166–76.
26. Li K, Wang Q, Bian B, Xu J, Bian H. Exploration and validation of the hub genes involved in hypoxia-induced endothelial-mesenchymal transition of systemic sclerosis. Clin Exp Rheumatol 2023.
27. Han Y, Li Z, Wu Q, Liu H, Sun Z, Wu Y, Luo J. B4GALT5 high expression associated with poor prognosis of hepatocellular carcinoma. BMC Cancer. 2022;22(1):392.
28. Parker BL, Thaysen-Andersen M, Fazakerley DJ, Holliday M, Packer NH, James DE. Terminal Galactosylation and Sialylation switching on membrane glycoproteins upon TNF-Alpha-Induced insulin resistance in adipocytes. Mol Cell Proteom. 2016;15(1):141–53.
29. Ren Z, Huang X, Lv Q, Lei Y, Shi H, Wang F, Wang M. High expression of B4GALT1 is associated with poor prognosis in acute myeloid leukemia. Front Genet. 2022;13:882004.
30. Sha YL, Liu Y, Yang JX, Wang YY, Gong BC, Jin Y, Qu TY, Xia FT, Han L, Zhao Q. B3GALT4 remodels the tumor microenvironment through GD2-mediated lipid raft formation and the c-met/AKT/mTOR/IRF-1 axis in neuroblastoma. J Exp Clin Cancer Res. 2022;41(1):314.

Publisher's note